A 21pJ/pulse FCC Compliant UWB Pulse Generator

Yousif Shamsa and Wouter A. Serdijn
Electronics Research Laboratory, Faculty of Electrical Engineering, Mathematics and Computer Science
Delft University of Technology, Mekelweg 4, 2628 CD Delft, the Netherlands
yousifshamsa@gmail.com, w.a.serdijn@tudelft.nl

***Abstract*—An LC filter based UWB pulse generator to be implemented in IBM 0.13 μm CMOS technology is presented. A 6^{th} order elliptical filter approximation of the Federal Communications Commission (FCC) Ultra Wide Band (UWB) mask is used to generate the transfer function. The filter order is chosen based on mask filling efficiency, component spread and circuit complexity. The impulse response of the filter is used to generate the UWB pulse. The current consumption is 2.8 mA at 1.5V, at a pulse rate of 200 MHz. The bandwidth of the UWB pulse is 4GHz. The pulse generator operates over the military temperature range (-40°C to 125°C). Monte Carlo analysis simulation results show an acceptable effect of both mismatch and process variations on the UWB pulse.**

I. Introduction

Ultra Wide Band (UWB) technology is gaining momentum since 2002, when the Federal Communications Commission (FCC) approved this technology for commercial applications [1], [2]. UWB promises great potential for high speed communication without exclusive frequency allocation [3]. Impulse-Radio UWB (IR-UWB) forms one of the possible candidates to implement UWB communication. IR-UWB utilizes very short transient pulses as information carriers, which results in a very wide frequency spectrum. The FCC has allocated a bandwidth of 7.5GHz (3.1-10.6 GHz) to UWB [4]. In this paper, an UWB pulse generator is proposed which is implemented using a new filter topology. The pulse generator has an peak voltage control circuit, which allows the generator to adjust the magnitude of the transmitted signal thereby ensuring FCC compliance. The pulse generator can be modulated by means of on-off keying. Because of the topology used, the effect of mismatch, process variations and temperature variations on the UWB pulse are minimal.

II. System Design

A. Filter Topologies

To maximize the signal to noise ratio (SNR) of the UWB wireless link, the radiated power has to be maximized. The effective isotropic radiated power (EIRP) is limited by the FCC by the UWB Emission Mask. To send a high power pulse, the pulse has to approximate the FCC mask shape as well as possible. Several approximation techniques exist: Padé approximation [5] and L2 approximation [6]. It is also possible to use a filter transfer function [7]. The UWB pulse used in this work is derived from a 6^{th} order elliptical filter approximation of the FCC mask. The order is chosen based on mask filling efficiency, circuit complexity and component spread. The transfer function is transformed into a state-space description using a numerical computing environment (MATLAB), as shown in Equations 1 and 2. Subsequently, the state-space description is transformed into an orthonormal ladder state-space representation. This system description has several advantages. First of all, the system has a low sensitivity to components variations. The sparsity of the A-matrix of the orthonormal ladder state-space forms another advantage. This decreases the number of elements needed to implement the system and thus decreases the complexity of the circuit. The final advantage of this description is the ability to transform it to an LC ladder and thus implement the system with passive elements which leads to lower power consumption [8]. The orthonormal ladder state-space representation is shown in Equations 5 and 6.

$$sX(s) = AX(s) + BU(s) \tag{1}$$
$$Y(s) = CX(s) + DU(s) \tag{2}$$

It is also possible to use differentiators instead of integrators. The differentiation based state-space description is shown in Equations 3 and 4. It is also possible to transform this description into an LC filter. The difference is that the integration based description can be transformed into a low-pass LC topology, whereas the differentiation based description can be transformed into a high-pass LC topology.

$$\frac{1}{s}X(s) = AX(s) + BU(s) \tag{3}$$
$$Y(s) = CX(s) + DU(s) \tag{4}$$

The LC ladder implements the A-matrix and the B-matrix of the state space description. The C-matrix implements a weighted addition of the states of the LC filter. The C-matrix factors are usually implemented using transconductance amplifiers. Due to the fact that C-matrix factors generally differ, different transconductance amplifiers have to be designed. To simplify the circuit design, the C-matrix factors can be implemented using passive elements as shown in Figures 1 and 2. From the two possibilities of LC filters, the low-pass topology is favored because of the higher Q-factor of floating inductors. This topology is also favored from a chip area point of view because of the lower number of inductors used.

The elliptic filter transfer function is shown in Equation 7. From the transfer function, the filter components are calculated using MATLAB.

978-1-4244-5309-2/10/$26.00 ©2010 IEEE

$$A = 1e9 \begin{bmatrix} 0 & 31.7 & 0 & 0 & 0 & 0 \\ -31.7 & 0 & 16.7 & 0 & 0 & 0 \\ 0 & -16.7 & 0 & 42.7 & 0 & 0 \\ 0 & 0 & -42.7 & 0 & 27.9 & 0 \\ 0 & 0 & 0 & -27.9 & 0 & 51 \\ 0 & 0 & 0 & 0 & -51 & -40.1 \end{bmatrix} \quad B = \begin{bmatrix} 0 \\ 0 \\ 0 \\ 0 \\ 0 \\ 1 \end{bmatrix} \tag{5}$$

$$C = \begin{bmatrix} 0 & -1.0 & 0 & 0.22 & 0 & 0.001 \end{bmatrix} \quad D = \begin{bmatrix} 0 \end{bmatrix} \tag{6}$$

$$H(s) = \frac{8.975e7\, s^5 + 2.065e5\, s^4 + 1.1e31\, s^3 + 1.255e26\, s^2 + 2.086e50\, s - 1.912e40}{s^6 + 3.623e10\, s^5 + 5.493e21\, s^4 + 1.212e32\, s^3 + 8.374e42\, s^2 + 8.422e52\, s + 3.544e63} \tag{7}$$

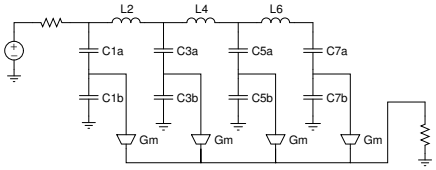

Fig. 1. Low-pass filter topology

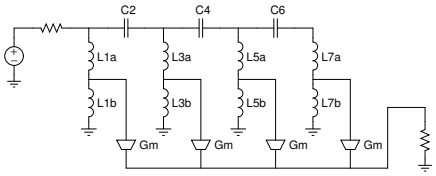

Fig. 2. High-pass filter topology

TABLE I
CIRCUIT COMPONENTS VALUES AND SPECIFICATIONS

Capacitors	C1	C2a	C2b	C3
Cell Name	mimcap	mimcap	mimcap	dualmimcap
Length	8.5u	8.5u	8.5u	8.5u
Width	6.28u	27.41u	98.71u	39.09u
Capacitance	114.07fF	488.9fF	1.75pF	2.49pF
Inductors	L1	L2	L3	
Cell Name	ind	ind	ind	
Dimension	190u	140u	100u	
n turns	4	3	1.75	
Inductance	3.374nH	1.431nH	404pH	
Transistors	NMOS	PMOS		
Cell Name	nfet	pfet		
Length	120n	120n		
Width	150u	450u		
Resistors	R1	R2		
Cell Name	kxres	kxres		
Length	5u	5u		
Width	5u	5u		
Resistance	63.7 Ohms	63.7 Ohms		

III. CIRCUIT DESIGN

The circuit consists of a clock driver, an impulse generator, an LC ladder and a read-out circuit. The clock driver consists of an inverter (consisting of M1 and M2). The impulse generator consists of a NAND stage, a delay and a NOR stage. The NAND (M3, M4, M5 and M6) has two inputs: the clock and the enable signal. Depending on the enable signal, the step is or is not applied to the next stage. Transistors M7 and M8 implement the delay element. Finally, the NOR stage (M10, M11, M12 and M13) mixes both the delayed and the non-delayed signals thereby generating an impulse. The generated impulse has a peak value of 0.8V and a duration of 100ps. Transistor M9 controls the supply current of the NOR stage. This, in turn, controls the peak voltage of the impulse and by this controls the peak-to-peak voltage of the UWB pulse. This peak voltage control allows for the use of this pulse generator with different UWB antenna gains. The read-out of the LC ladder is an implementation of the C-matrix. In case of a band-pass filter, the C-matrix consists of non-zero elements only on the even or the odd positions. For our 6^{th} order filter, the C-matrix consists of three elements -1, 0.22 and 0.001. However, the latter element is negligible. Thus, only the two non-negligible elements with opposite polarities have to be implemented. This makes it possible to connect a (50 Ω) UWB differential antenna directly to the output of the pulse generator without additional circuitry. The capacitances C2b and C3 can be partly absorbed into the bond pad of the chip. The total circuit is shown in Figure 3. The values of the circuit components are shown in Table I.

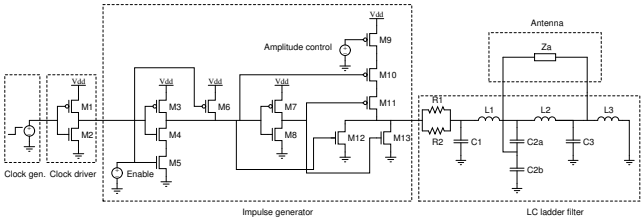

Fig. 3. The total circuit

IV. SIMULATION RESULTS

The generated UWB pulse over the military temperature range is shown in Figure 4. The peak to peak voltage (Vpp) of the pulse is 230 mV, while the duration is approximately 1 ns. Temperature variations cause a small variation in the peak-to-peak value of the UWB pulse, while the shape remains

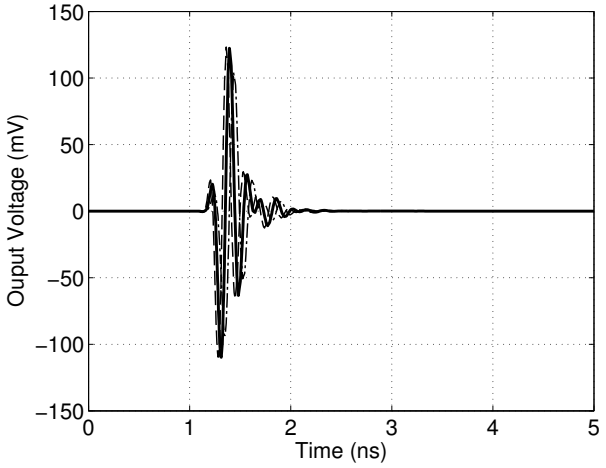

Fig. 4. Effect of temperature variation on the UWB pulse

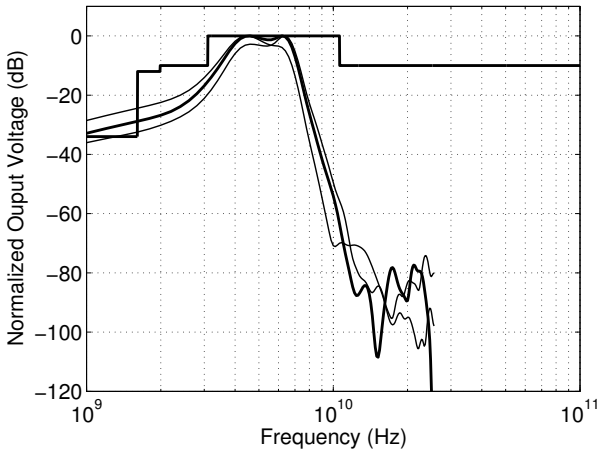

Fig. 5. Effect of temperature variation on the normalized PSD of the UWB pulse

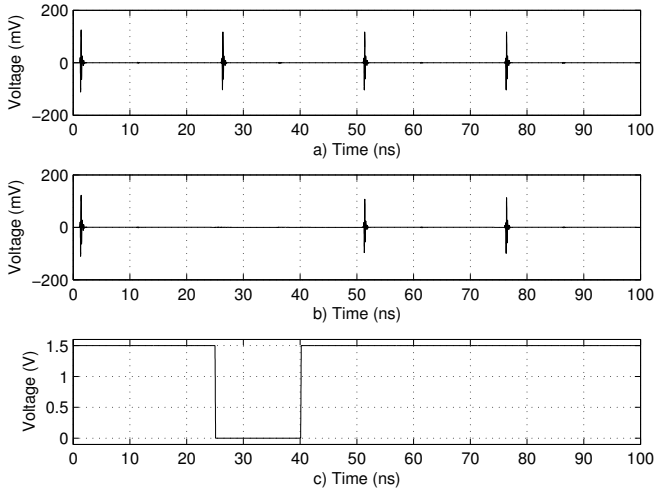

Fig. 6. Pulse generator on-off keying. a) enable signal always high ("1"), b) on-off keyed signal, c) enable signal

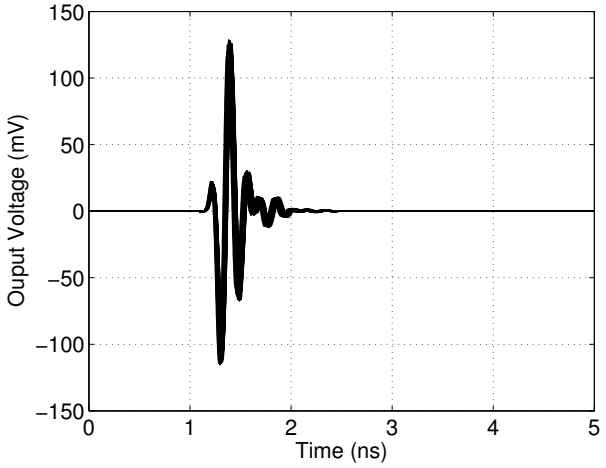

Fig. 7. Effect of mismatch and process variations on the UWB pulse

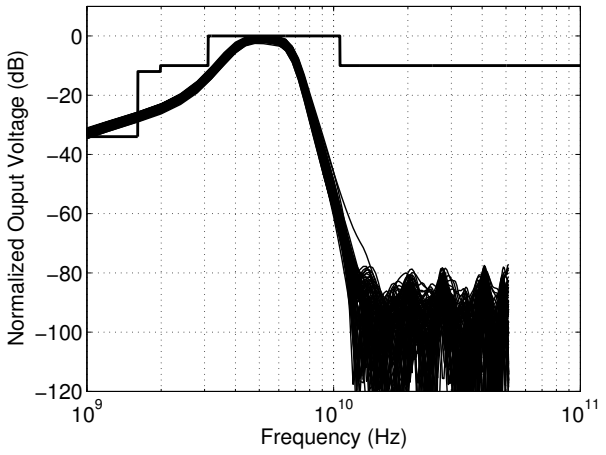

Fig. 8. Effect of mismatch and process variations on the normalized PSD of the UWB pulse

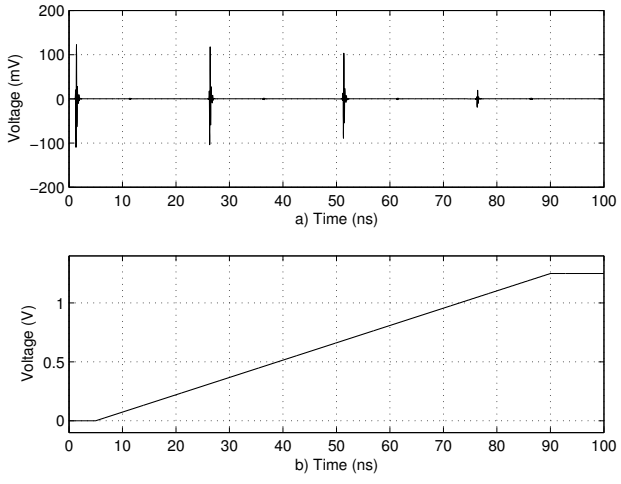

Fig. 9. Pulse generator peak-to-peak voltage control. a) generated output pulse, b) control signal

unchanged. In Figure 5, the Power Spectral Density (PSD) of the UWB pulse is shown over the military temperature range (-40°C to 125°C). The PSD is compliant with the FCC mask except in the "GPS region" (960-1610 MHz). This forms no problem because of the bandwidth of the antenna. The bandwidth of the UWB pulse is 4 GHz.

The effect of mismatch and process variations on both the UWB pulse and its PSD are simulated using a Monte Carlo analysis (100 iterations). The results are shown in Figures 8 and 7. The UWB pulse is relatively insensitive to both mismatch and process variations.

Transistor M9 controls the supply current to the NOR stage of the impulse generator. By applying a signal on M9 the peak-to-peak value of the UWB pulses is controlled. Figure 9a shows pulses with different peak-to-peak values as a result of a ramp signal on the gate of M9, as shown in 9b.

The NAND stage of the impulse generator applies the step input to the next stage depending on the enable signal. When the enable signal is equal to zero, no pulse is generated. In Figure 6a the pulses are shown as a result of an enable signal equal to "1". Figure 6b shows that the second pulse is blocked by the enable signal going to "0" as shown in Figure 6c.

V. Conclusion

An UWB pulse generator to be implemented in IBM 0.13 μm CMOS technology is presented. A 6^{th} order elliptical filter approximation is used to generate the transfer function. Subsequently, the transfer function is transformed into an LC filter. The complete circuit consists of an impulse generator and an LC ladder. The peak value can be controlled using supply current control of the last stage. This allows for FCC mask compliance even in extreme conditions. The pulse generator has a -10dB bandwidth of 4GHz and a current consumption of 2.8mA at 1.5V, at a pulse rate of 200MHz. The effects of components mismatch and process variations are acceptable, according to Monte Carlo analyses. Simulation results over the military temperature range (-40°C to 125°C) show an acceptable variation of the UWB pulse in both time and frequency domain. In Table II, the pulse generator performance is summarized. Table III gives the performance summary of this design in comparison with previous work.

TABLE II
Design performances

Specifications	This Work
Frequency mask	Elliptical filter
BW(-10 dB)	4 GHz
Current cons.	2.8mA @ 1.5V @ 200MHz
Energy cons.	21pJ/pulse
Vpp @ 50 Ω	230 mV
Pulse width	1 ns
Process	IBM 0.13 μm CMOS
Type of input signal	Binary clock/enable
Temperature range	-40°C to 125°C

TABLE III
Pulse generator circuit performance comparison

	Ref. [9]	Ref. [10]	Ref. [11]	This Work
Vpp @ 50 Ω	1,24V	0,16V	1,0V	0,23V
Power cons.	29,7mW	1,68mW	2,7mW	4,2mW
	@36MHz	@100MHz	@200MHz	@200MHz
BW (-10 dB)	1,4GHz	520MHz	4,3GHz	4.0 GHz
Pulse width	1,75ns	3,5ns	0,6ns	1,0 ns
Process	CMOS 0,18μ	CMOS 0,18μ	CMOS 0,13μ	CMOS 0,13μ

References

[1] First Report and Order, FCC 02-48, Federal Communications Commission, ET Docket 98-153, February 2002.

[2] Second Report and Order and Second Memorandum Opinion and Order, FCC 04-285, Federal Communications Commission, ET Docket 98-153, December 2004.

[3] Porcino, D.; Hirt, W., "Ultra-wideband radio technology: potential and challenges ahead," Communications Magazine, IEEE, vol.41, no.7, pp. 66-74, July 2003

[4] R. Fisher, R. Kohno, M. McLaughlin, and M. Welbourn, DS-UWB Physical Layer Submission to IEEE 802.15 Task Group 3a (Doc. Number P802.15-04/0137r4), IEEE P802.15, Jan. 2005.

[5] Haddad, S.A.P.; Verwaal, N.; Houben, R.; Serdijn, W.A., "Optimized dynamic translinear implementation of the Gaussian wavelet transform," Circuits and Systems, 2004. ISCAS '04. Proceedings of the 2004 International Symposium on, vol.1, pp. I-145-I-148 Vol.1, 23-26 May 2004

[6] Sandro A.P. Haddad and Wouter A. Serdijn: Ultra Low-Power Biomedical Signal Processing: an analog wavelet filter approach for pacemakers, Springer, 2009, ISBN:978-1-4020-9072-1.

[7] S. Bagga, S.A.P. Haddad, Koen van Hartingsveldt, Simon Lee and W.A. Serdijn, "An Interference Rejection Filter For An Ultra-Wideband Quadrature Downconversion Autocorrelation Receiver," in *Proceedings IEEE International Symposium of Circuits and Systems*, May 2005

[8] Johns, D.A.; Snelgrove, W.M.; Sedra, A.S., "Orthonormal ladder filters," Circuits and Systems, IEEE Transactions on, vol.36, no.3, pp.337-343, Mar 1989

[9] Norimatsu, T.; Fujiwara, R.; Kokubo, M.; Miyazaki, M.; Maeki, A.; Ogata, Y.; Kobayashi, S.; Koshizuka, N.; Sakamura, K., "A UWB-IR Transmitter With Digitally Controlled Pulse Generator," Solid-State Circuits, IEEE Journal of, vol.42, no.6, pp.1300-1309, June 2007

[10] Anh Tuan Phan; Jeongseon Lee; Krizhanovskii, V.; Quan Le; Seok-Kyun Han; Sang-Gug Lee, "Energy-Efficient Low-Complexity CMOS Pulse Generator for Multiband UWB Impulse Radio," Circuits and Systems I: Regular Papers, IEEE Transactions on, vol.55, no.11, pp.3552-3563, Dec. 2008

[11] Bourdel, S.; Gaubert, J.; Fourquin, O.; Vauche, R.; Dehaese, N., "CMOS UWB pulse generator co-designed with package transition," Radio Frequency Integrated Circuits Symposium, 2009. RFIC 2009. IEEE, pp.539-542, 7-9 June 2009